

REDUCTION OF SPURIOUS VELOCITY
IN FINITE DIFFERENCE LATTICE BOLTZMANN MODELS
FOR LIQUID - VAPOR SYSTEMS

Artur CRISTEA and Victor SOFONEA*

*Laboratory for Numerical Simulation and Parallel Computing in Fluid Mechanics
Center for Fundamental and Advanced Technical Research, Romanian Academy
Bd. Mihai Viteazul 24, R – 1900 Timișoara, Romania*

E-mail: {flastra,sofonea}@acad-tim.utt.ro

September 29, 2018

Abstract

The origin of the spurious interface velocity in finite difference lattice Boltzmann models for liquid - vapor systems is related to the first order upwind scheme used to compute the space derivatives in the evolution equations. A correction force term is introduced to eliminate the spurious velocity. The correction term helps to recover sharp interfaces and sets the phase diagram close to the one derived using the Maxwell construction.

Keywords: Lattice Boltzmann; Liquid - Vapor Systems; Spurious Interface Velocity.

1. General description of Finite Difference Lattice Boltzmann models

Lattice Boltzmann (LB) models [1, 2, 3, 4] provide an alternative to current simulation methods in computational fluid dynamics. These models are based on the physics at the mesoscopic scale, so that the macroscopic phenomena are recovered without solving the equations of continuous media mechanics. The starting point of any LB model is the Boltzmann equation [5]

$$\left(\frac{\partial}{\partial t} + \mathbf{v} \cdot \nabla + \frac{\mathbf{F}}{m} \cdot \nabla_{\mathbf{v}} \right) f = \left(\frac{\partial f}{\partial t} \right)_{collisions} \quad (1)$$

*Corresponding author.

Here $f \equiv f(\mathbf{r}, \mathbf{v}, t)$ is the distribution function of fluid particles (supposed to be identical, with mass m), \mathbf{v} is the particle velocity and $\mathbf{F} = \mathbf{F}(\mathbf{r}, t)$ is the local force acting on fluid particles. The collision term in the Boltzmann equation (1) is usually linearized using the Bhatnagar-Gross-Krook (BGK) approximation [6] after introducing a relaxation time τ :

$$\left(\frac{\partial f}{\partial t} \right)_{\text{collisions}} = -\frac{1}{\tau} [f(\mathbf{r}, \mathbf{v}, t) - f^{eq}(\mathbf{r}, \mathbf{v}, t)] \quad (2)$$

The equilibrium distribution function $f^{eq} \equiv f^{eq}(\mathbf{r}, \mathbf{v}, t)$ which appears in eq. (2) is the Maxwell - Boltzmann distribution function:

$$f^{eq}(\mathbf{r}, \mathbf{v}, t) = n(\mathbf{r}, t) \left(\frac{m}{2\pi k_B T} \right)^{1/2} \exp \left\{ -\frac{m}{2k_B T} \cdot [\mathbf{v} - \mathbf{u}(\mathbf{r}, t)]^2 \right\} \quad (3)$$

where k_B is the Boltzmann constant, T is the absolute temperature of the system,

$$n(\mathbf{r}, t) = \int f(\mathbf{r}, \mathbf{v}, t) d\mathbf{v} \quad (4)$$

is the particle number density and

$$\mathbf{u}(\mathbf{r}, t) = \frac{1}{n(\mathbf{r}, t)} \int \mathbf{v} \cdot f(\mathbf{r}, \mathbf{v}, t) d\mathbf{v} \quad (5)$$

is the local fluid velocity [7]. We assume that the system is not too far from the equilibrium state and get [8, 9]

$$\nabla_{\mathbf{v}} f(\mathbf{r}, \mathbf{v}, t) \simeq \nabla_{\mathbf{v}} f^{eq}(\mathbf{r}, \mathbf{v}, t) = -\frac{m}{k_B T} [\mathbf{v} - \mathbf{u}(\mathbf{r}, t)] f^{eq}(\mathbf{r}, \mathbf{v}, t) \quad (6)$$

Recent investigations [10, 11, 12] resulted in a general procedure to construct lattice Boltzmann models for single - component fluids. After discretization of the phase space [1, 2, 3, 4], the distribution functions are defined only in the nodes \mathbf{x} of a discrete lattice \mathcal{L} in the one - (1D), two - (2D) or three - dimensional (3D) space, while the velocities are reduced to a discrete set $\{\mathbf{e}_i\}$, $i = 0, 1, \dots, \mathcal{N}$. The elements of the 1D, 2D and 3D velocity sets $\{\mathbf{e}_i\}$ currently used in the LB literature [3, 4, 10, 13] are expressed using the propagation speed $c = \sqrt{k_B T / \chi m}$, where χ is a constant specific to each set. Following the discretization procedure, the Boltzmann equation (1) is replaced by the set of \mathcal{N} equations

$$\begin{aligned} \partial_t f_i(\mathbf{x}, t) + \mathbf{e}_i \cdot \nabla f_i(\mathbf{x}, t) &= -\frac{1}{\tau} [f_i(\mathbf{x}, t) - f_i^{eq}(\mathbf{x}, t)] \\ &+ \frac{1}{\chi c^2} f_i^{eq}(\mathbf{x}, t) [\mathbf{e}_i - \mathbf{u}(\mathbf{x}, t)] \cdot \mathbf{F}(\mathbf{x}, t) \\ (i = 0, 1, \dots, \mathcal{N}) & \end{aligned} \quad (7)$$

where the distribution functions $f_i(\mathbf{x}, t)$ express the probability of finding at node $\mathbf{x} \in \mathcal{L}$ a particle having the velocity \mathbf{e}_i . The particle number density n and the local velocity \mathbf{u} are now expressed as

$$n = n(\mathbf{x}, t) = \sum_{i=0}^{i=\mathcal{N}} f_i(\mathbf{x}, t) = \sum_{i=0}^{i=\mathcal{N}} f_i^{eq}(\mathbf{x}, t) \quad (8)$$

$$\mathbf{u} = \mathbf{u}(\mathbf{x}, t) = \frac{1}{n(\mathbf{x}, t)} \sum_{i=0}^{i=\mathcal{N}} \mathbf{e}_i f_i(\mathbf{x}, t) = \frac{1}{n(\mathbf{x}, t)} \sum_{i=0}^{i=\mathcal{N}} \mathbf{e}_i f_i^{eq}(\mathbf{x}, t) \quad (9)$$

while the equilibrium distribution functions in (7) are given as series expansion in the local velocity:

$$f_i^{eq} = f_i^{eq}(\mathbf{x}, t) = w_i n \left[1 + \frac{\mathbf{e}_i \cdot \mathbf{u}}{\chi c^2} + \frac{(\mathbf{e}_i \cdot \mathbf{u})^2}{2\chi^2 c^4} - \frac{\mathbf{u} \cdot \mathbf{u}}{2\chi c^2} \right] \quad (10)$$

In the one - dimensional $D1Q3$ model [4], $\chi = 1/3$, $\mathcal{N} = 2$ and the velocities \mathbf{e}_i are given by:

$$\mathbf{e}_i = \begin{cases} 0 & (i = 0) \\ c & (i = 1) \\ -c & (i = 2) \end{cases} \quad (11)$$

while the weight factors w_i in (10) are

$$w_i = \begin{cases} 4/6 & (i = 0) \\ 1/6 & (i = 1, 2) \end{cases} \quad (12)$$

When using a square lattice in the 2D space (D2Q9 model [14]), $\chi = 1/3$, $\mathcal{N} = 8$ and the velocities \mathbf{e}_i are given by

$$\mathbf{e}_i = \begin{cases} 0 & (i = 0) \\ \left[\cos \frac{(i-1)\pi}{2}, \sin \frac{(i-1)\pi}{2} \right] c & (i = 1, \dots, 4) \\ \left[\cos \left(\frac{\pi}{4} + \frac{(i-5)\pi}{2} \right), \sin \left(\frac{\pi}{4} + \frac{(i-5)\pi}{2} \right) \right] \sqrt{2} c & (i = 5, \dots, 8) \end{cases} \quad (13)$$

while the weight factors are

$$w_i = \begin{cases} 4/9 & (i = 0) \\ 1/9 & (i = 1, \dots, 4) \\ 1/36 & (i = 5, \dots, 8) \end{cases} \quad (14)$$

The Cartesian projections $e_{i\alpha} \equiv (\mathbf{e}_i)_\alpha$ ($i = 1, 2, \dots, \mathcal{N}$; $\alpha = x, y, \dots$) of the velocity vectors \mathbf{e}_i satisfy the relations

$$\begin{aligned}
\sum_i w_i e_{i\alpha} &= 0 \\
\sum_i w_i e_{i\alpha} e_{i\beta} &= \chi c^2 \delta_{\alpha\beta} \\
\sum_i w_i e_{i\alpha} e_{i\beta} e_{i\gamma} &= 0 \\
\sum_i w_i e_{i\alpha} e_{i\beta} e_{i\gamma} e_{i\delta} &= \chi^2 c^4 (\delta_{\alpha\beta} \delta_{\gamma\delta} + \delta_{\beta\gamma} \delta_{\delta\alpha} + \delta_{\alpha\gamma} \delta_{\beta\delta}) \quad (15)
\end{aligned}$$

The following sums are easily computed using the definition (10) of the equilibrium distribution functions:

$$\begin{aligned}
\sum_i f_i^{eq} &= n \\
\sum_i e_{i\alpha} f_i^{eq} &= n u_\alpha \\
\sum_i e_{i\alpha} e_{i\beta} f_i^{eq} &= n [\chi c^2 \delta_{\alpha\beta} + u_\alpha u_\beta] \\
\sum_i e_{i\alpha} e_{i\beta} e_{i\gamma} f_i^{eq} &= n \chi c^2 [\delta_{\alpha\beta} u_\gamma + \delta_{\beta\gamma} u_\alpha + \delta_{\gamma\alpha} u_\beta] \quad (16)
\end{aligned}$$

Here u_α ($\alpha = x, y$) are the Cartesian components of the local velocity \mathbf{u} .

The set of phase space discretized LB equations (7) for the distribution functions $f_i = f_i(\mathbf{x}, t)$ may be solved numerically using an appropriate finite difference scheme defined on the lattice \mathcal{L} . When using a scheme based on the characteristics line, the forward Euler difference is used to compute the time derivative while the first - order upwind scheme may be used for the space derivative [13] as usually done in classical LB models [3, 4]. These schemes give the following updating procedure for the distribution function [13, 15, 16]

$$\begin{aligned}
f_i(\mathbf{x}, t + \delta t) &= f_i(\mathbf{x}, t) + \frac{c\delta t}{\delta s} [f_i(\mathbf{x}, t) - f_i(\mathbf{x} - \delta s \mathbf{e}_i/c, t)] \\
&\quad - \frac{\delta t}{\tau} [f_i(\mathbf{x}, t) - f_i^{eq}(\mathbf{x}, t)] + \frac{\delta t}{\chi c^2} f_i^{eq}(\mathbf{x}, t) [\mathbf{e}_i - \mathbf{u}(\mathbf{x}, t)] \cdot \mathbf{F}(\mathbf{x}, t) \quad (17)
\end{aligned}$$

where δt is the time step and δs is the lattice spacing.

2. Dimensionless equations and the force term

Let l_R , t_R , n_R , T_R , c_R and a_R the reference quantities for length, time, particle number density, temperature, speed and acceleration. In order to preserve the

form (7) of the LB evolution equations, the reference quantities should satisfy the following relations

$$\begin{aligned}\frac{t_R c_R}{l_R} &= 1 \\ \frac{a_R t_R}{c_R} &= 1\end{aligned}\tag{18}$$

Since we will refer further to a van der Waals fluid, a natural choice for n_R , T_R and c_R may be the values corresponding to a mole of fluid at the critical point [17], $n_R = N_A/V_{mc}$, $T_R = T_c$ and $c_R = \sqrt{k_B T_c/m}$, respectively. Here N_A is Avogadro's number, V_{mc} is the molar volume at the critical point and T_c is the critical temperature. With this choice of the reference quantities, the dimensionless propagation speed is

$$c = \sqrt{T/\chi}\tag{19}$$

where T is the dimensionless temperature (note that $T = 1$ at the critical point). The other reference quantities may be derived from Eqs. (18). if we choose the characteristic system size as reference length.

The fact that the dimensionless propagation velocity c (19) should not necessarily equal 1 is a characteristics of the Finite Difference LB models [18], where the propagation velocity is no longer related to the lattice spacing as in standard (classical) LB models [3, 4]. Comparison of fluid velocity profiles at different temperatures becomes easier with the definition (19) associated to the expression (9) of the local fluid velocity.

The local force acting on a fluid particle is the sum of two terms:

$$\mathbf{F}(\mathbf{x}, t) = \mathbf{F}^\varphi + \mathbf{F}^\sigma\tag{20}$$

The first term \mathbf{F}^φ accounts for phase separation in the van der Waals fluid, while the second one \mathbf{F}^σ generates the surface tension at the interface between phases. The expression of \mathbf{F}^φ and \mathbf{F}^σ is adopted from the literature [9]

$$\mathbf{F}^\varphi = \frac{1}{\rho} \nabla (-p_w + \chi c^2 \rho)\tag{21}$$

$$\mathbf{F}^\sigma = \kappa \nabla (\nabla^2 \rho)\tag{22}$$

Here p_w is the van der Waals pressure, $\chi c^2 \rho$ is the dimensionless pressure of the ideal gas and κ is a parameter that controls the surface tension. When using the reference pressure $p_R = m n_R c_R^2$, which is in accordance to Eqs. (18), the dimensionless van der Waals equation of state reads

$$p_w = \frac{\rho T}{3 - \rho} - \frac{3}{8} \rho^2\tag{23}$$

Note that the dimensionless form (23) of the van der Waals equation of state is different from the form used by other authors [19, 20].

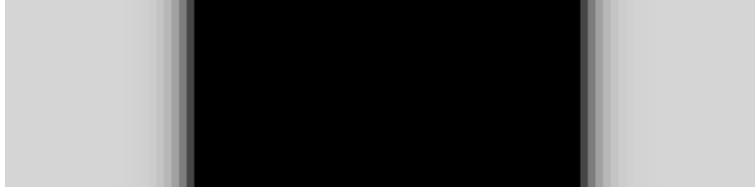


Figure 1: Plane interfaces in a $2D$ liquid - vapor system (the high density phase is black). Lattice size: 100×25 nodes; lattice spacing: $\delta s = 0.01$; time spacing: $\delta t = 0.001$; temperature: $T = 0.70$; surface tension parameter: $k = 0.00005$.

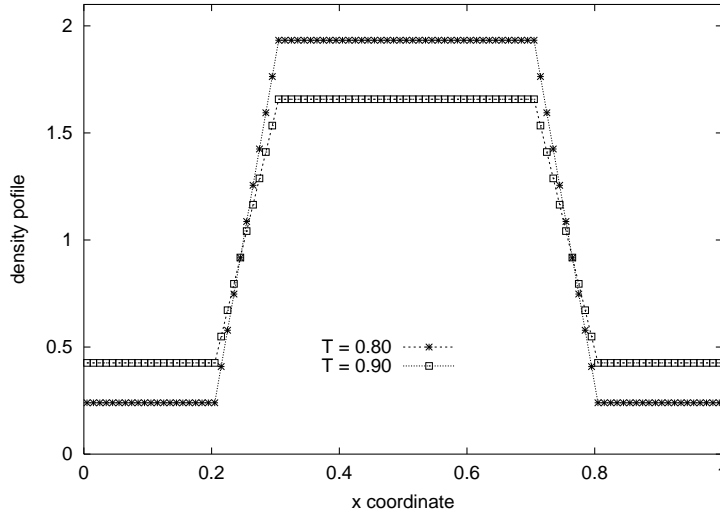


Figure 2: Initial density profiles for two values of the dimensionless temperature.

3. Stationary case: origin of the spurious velocity in the interface region

Simulation results reported in this paper refer to the equilibrium state of flat interfaces in liquid - vapor systems like the $2D$ one shown in Figure 1. Density, velocity and pressure profiles, as well as the phase diagram recovered in the stationary (equilibrium) state are found to be identical when using both $D1Q3$ and $D2Q9$ models. For this reason, we refer to the $D1Q3$ model on a $1D$ lattice with $N = 100$ nodes (i.e., $\delta s = 0.01$) when reporting the simulation results, as follows.

For each value of the temperature, the initial density profile was set up to allow a transition region (Figure 2), while the values of the initial density of the liquid and vapor phases were computed using the Maxwell construction [17]. This procedure (which avoids large density gradients) helps the system to exhibit a stable behavior

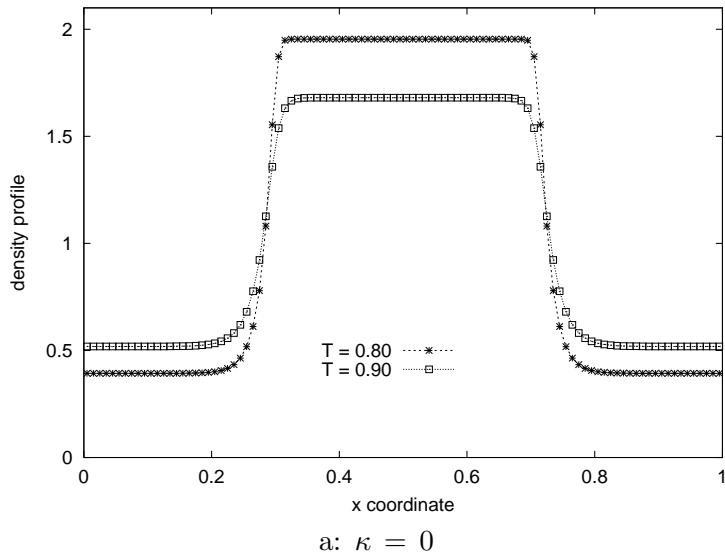
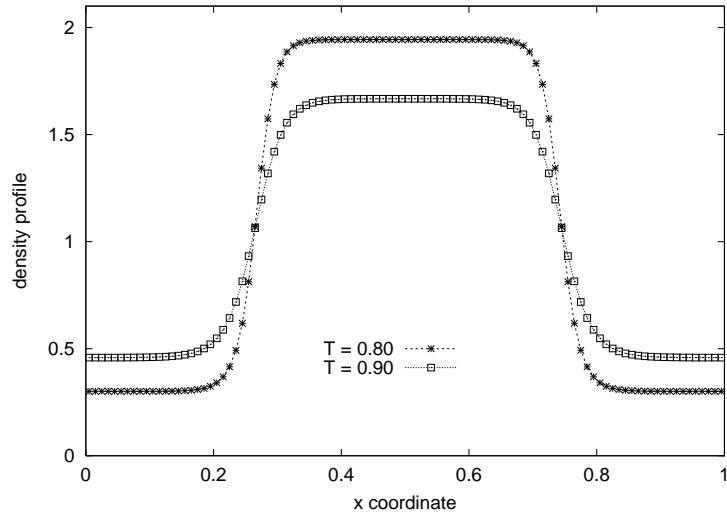


Figure 3: Equilibrium density profiles recovered with the first - order upwind scheme (17) for two values of the dimensionless temperature and different values of the surface tension parameter κ .

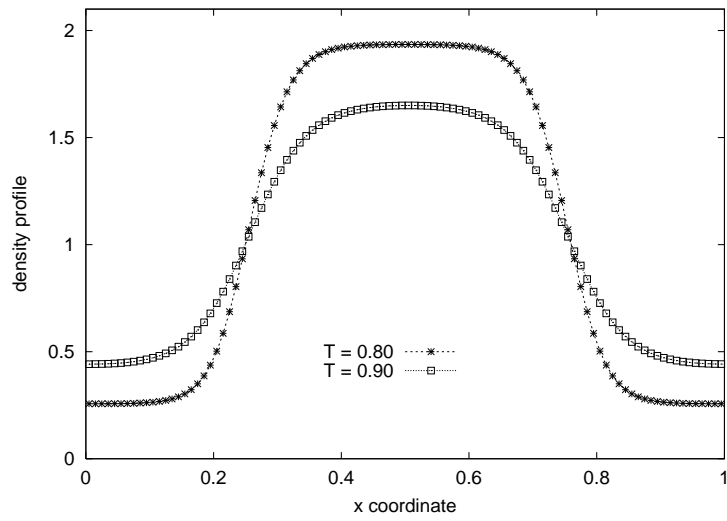
until the equilibrium state is reached. The dimensionless relaxation time was set to $\tau = 0.01$ and we always performed 200,000 time steps ($\delta t = 0.001$) using the upwind finite difference scheme (17) to ensure the equilibrium state of the fluid system.

Simulations were done with three values of the parameter κ which controls the surface tension. Figure 3 shows the resulting density profiles, for $T = 0.90$ and $T = 0.80$. As expected [19, 20], the interface width becomes larger as κ increases. But there is still a transition region between the two phases for $\kappa = 0$, when one would expect a sharp interface. Velocity profiles derived in the equilibrium state (Figure 4) show the existence of the spurious velocity (i.e., unphysical nonvanishing values of this quantity) in the interface region. The magnitude of the spurious velocity becomes larger when decreasing the temperature i.e., when the difference between the high and low density phases increases. However, the spurious velocity in the interface region reduces for larger values of the surface tension parameter κ , when density gradients in the interface region become smaller. Also, the interface profiles of the van der Waals pressure (23) shown in Figure 5 become wider when the value of κ is increased. For temperatures near the critical point and large values of κ , the left and right interfaces overlap one another. This is especially seen in Figure 5c, where the pressure plateaux of both the high and low density phase vanish for $T = 0.90$.

The phase diagram of the liquid vapor system (Figure 6) is strongly affected by



b: $\kappa = 0.00002$



c: $\kappa = 0.0001$

Figure 3: (*cont'd*) Equilibrium density profiles recovered with the first - order upwind scheme (17) for two values of the dimensionless temperature and different values of the surface tension parameter κ .

the value of the surface tension parameter κ . The liquid - vapor system becomes more stable (i.e., lower temperature states may be reached) when using larger values of κ which ensures smaller density gradients in the interface region. Moreover, when κ is increased, the computed values of the densities (especially in the vapor phase) become closer to the theoretical values derived using the Maxwell construction. The phase diagram becomes flawed near the critical point for larger κ , but this is an effect of the overlapping of the right and left interfaces.

To account for the spurious interface velocity, we recall that the *real* LB equations [13] solved using the upwind finite difference scheme in the stationary case are, up to second order in the lattice spacing δs

$$\begin{aligned} \mathbf{e}_i \cdot \nabla f_i(\mathbf{x}, t) - \psi e_{i\beta} e_{i\gamma} \partial_\beta \partial_\gamma f_i(\mathbf{x}, t) &= -\frac{1}{\tau} [f_i(\mathbf{x}, t) - f_i^{eq}(\mathbf{x}, t)] \\ &+ \frac{1}{\chi c^2} f_i^{eq} [e_{i\beta} - u_\beta(\mathbf{x}, t)] \cdot F_\beta(\mathbf{x}, t) \\ &(i = 0, 1, \dots, \mathcal{N}) \end{aligned} \quad (24)$$

where $\psi = \delta s / c$. Consequently, the stationary mass and momentum equations recovered from Eqs. (24) using the Chapman - Enskog procedure up to second order in the Knudsen number, are

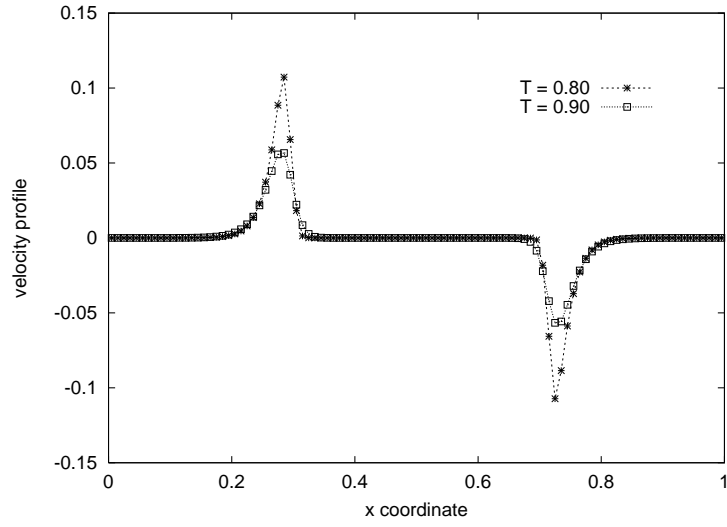
$$\partial_\beta(\rho u_\beta) = \psi \partial_\beta \partial_\gamma [\chi c^2 \rho \delta_{\beta\gamma} + \rho u_\beta u_\gamma] \quad (25)$$

$$\begin{aligned} \partial_\beta(\rho u_\alpha u_\beta) + \partial_\alpha p_w &= \chi c^2 \tau \partial_\beta [\rho \partial_\alpha u_\beta + \rho \partial_\beta u_\alpha] \\ &+ \chi c^2 \psi [2\partial_\alpha \partial_\beta(\rho u_\beta) + \nabla^2(\rho u_\alpha)] + \rho \kappa \partial_\alpha(\nabla^2 \rho) \end{aligned} \quad (26)$$

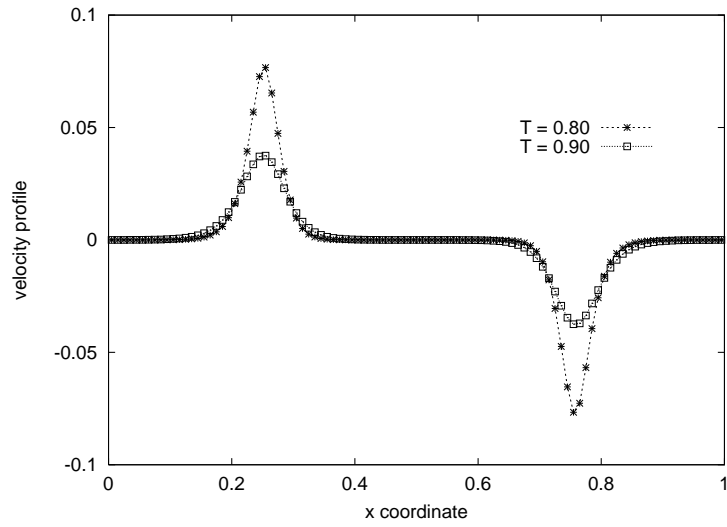
From the mass equation (25) we get the expression of the spurious velocity which is present in the interface region where the fluid density is not constant:

$$u_\beta = \frac{\psi}{\rho} \partial_\gamma [\chi c^2 \rho \delta_{\beta\gamma} + \rho u_\beta u_\gamma] \simeq \frac{\chi c^2 \psi}{\rho} \partial_\beta \rho \quad (27)$$

Thus, the spurious velocity is related to the numerical error introduced by the first order upwind finite difference scheme. Eq. (27) is in good agreement with simulation results (Figure 7), especially when the system temperature is near the critical point or when the surface tension parameter κ is large, i.e., when density gradients and the magnitude of the spurious velocity in the interface region are small.



a: $\kappa = 0$



b: $\kappa = 0.00002$

Figure 4: Equilibrium velocity profiles recovered with the first - order upwind scheme (17) for two values of the dimensionless temperature and different values of the surface tension parameter κ .

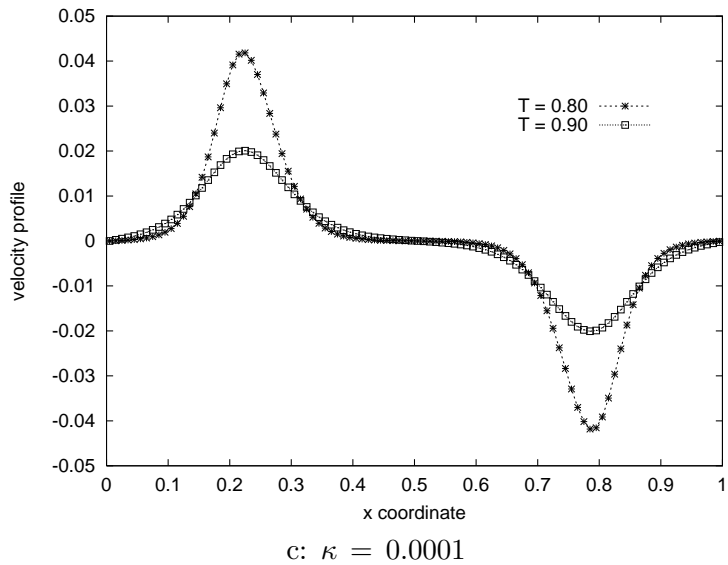


Figure 4: (*cont'd*) Equilibrium velocity profiles recovered with the first - order upwind scheme (17) for two values of the dimensionless temperature and different values of the surface tension parameter κ .

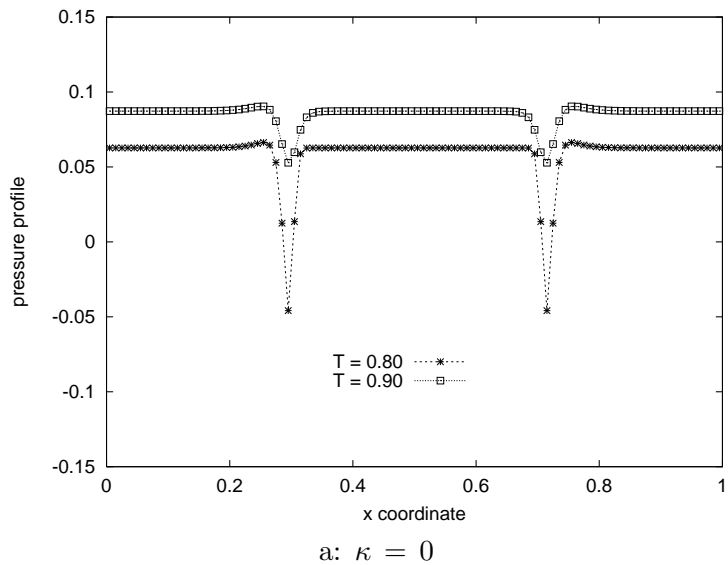
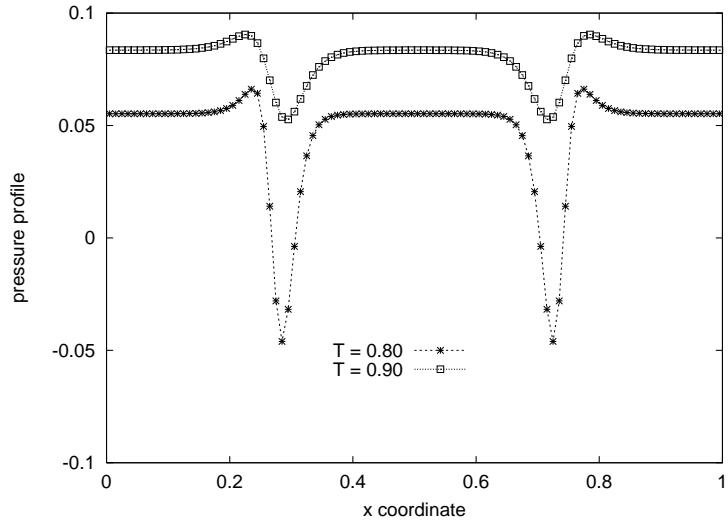
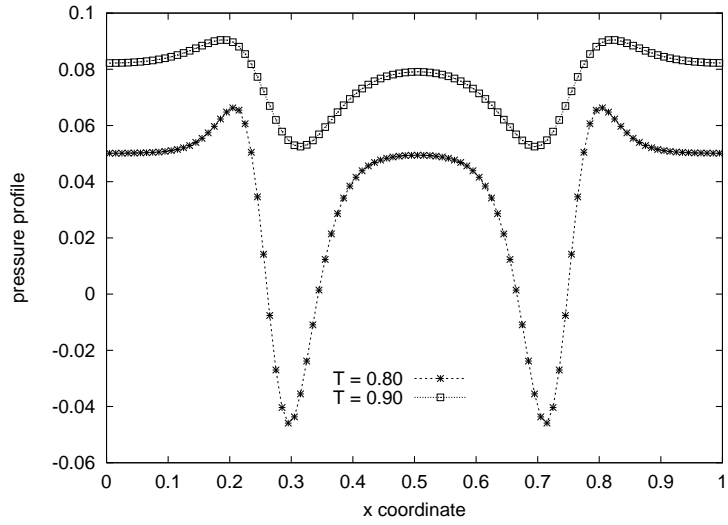


Figure 5: Equilibrium pressure profiles recovered with the first - order upwind scheme (17) for two values of the dimensionless temperature and different values of the surface tension parameter κ .

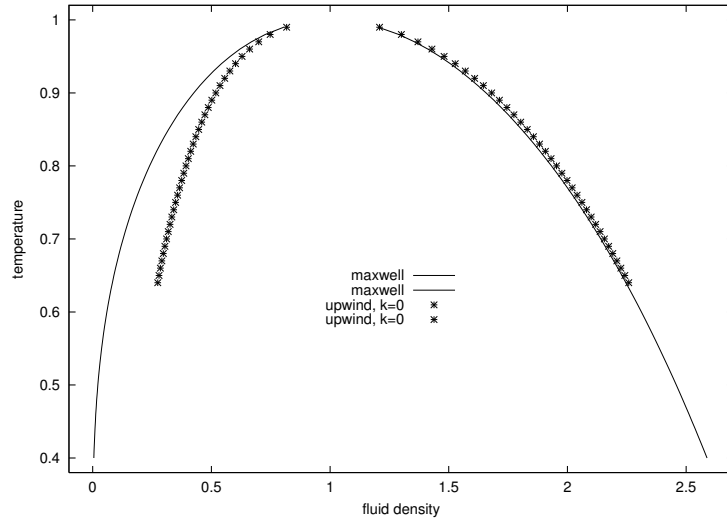


b: $\kappa = 0.00002$

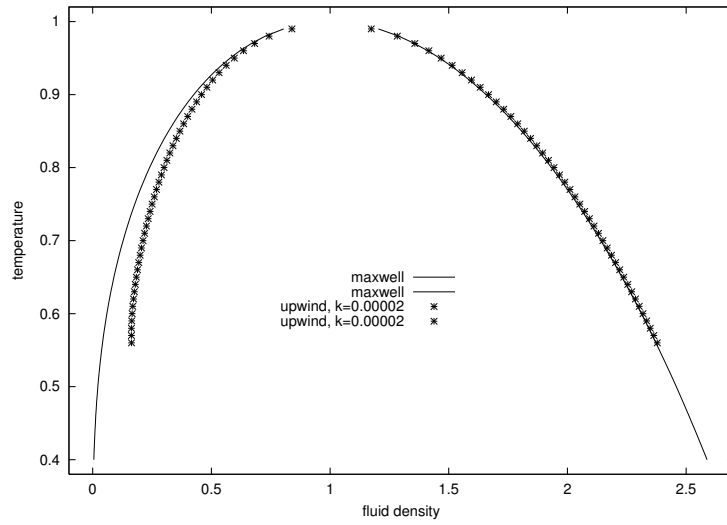


c: $\kappa = 0.0001$

Figure 5: (*cont'd*) Equilibrium pressure profiles recovered with the first - order upwind scheme (17) for two values of the dimensionless temperature and different values of the surface tension parameter κ .



a: $\kappa = 0$



b: $\kappa = 0.00002$

Figure 6: Phase diagrams recovered with the first - order upwind scheme (17) for different values of the surface tension parameter κ .

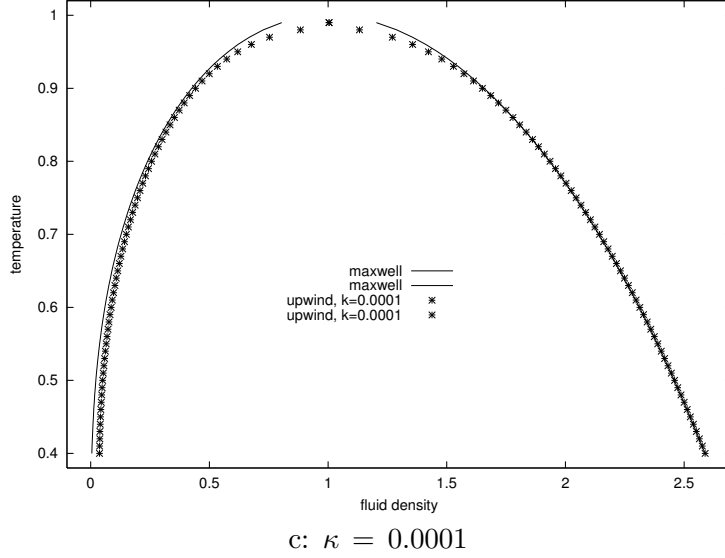


Figure 6: (*cont'd*) Phase diagrams recovered with the first - order upwind scheme (17) for different values of the surface tension parameter κ .

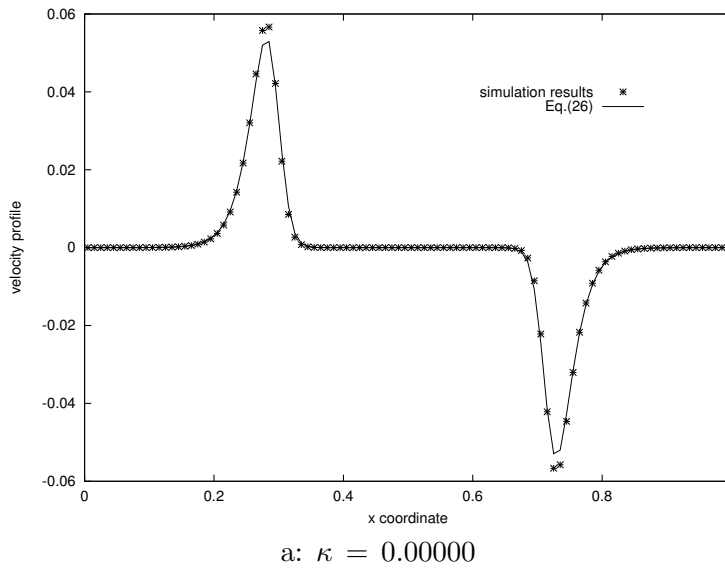
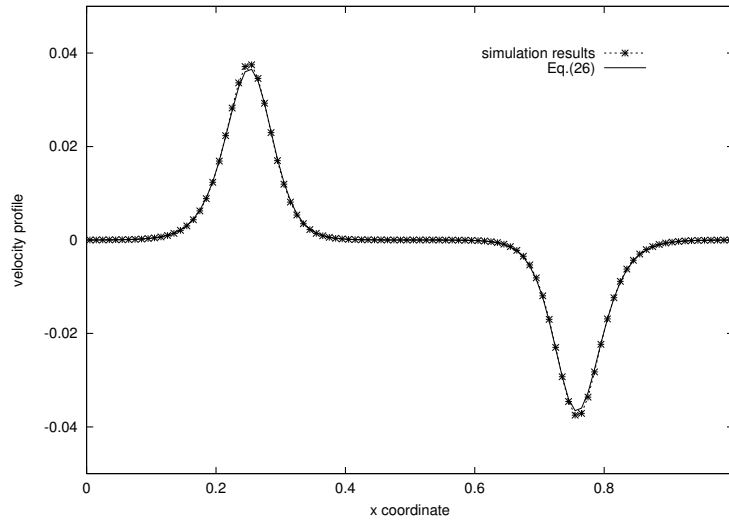
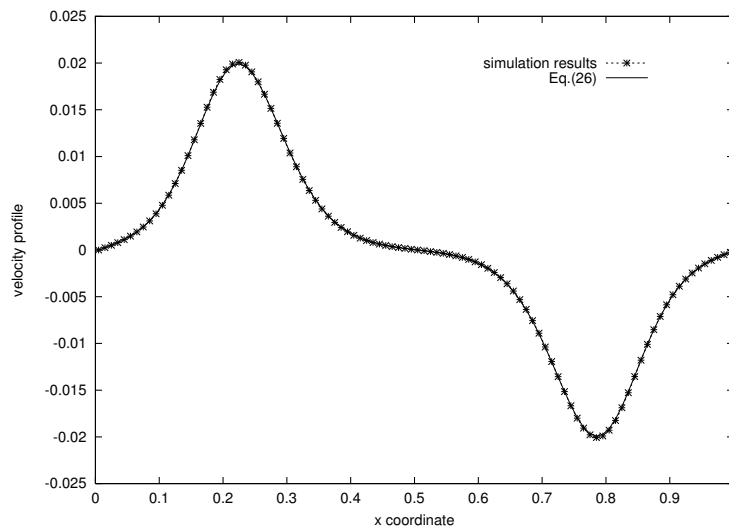


Figure 7: Velocity profile at $T = 0.90$: comparison between numerical results and Eq. (27) for different values of the surface tension parameter κ .



b: $\kappa = 0.00002$



c: $\kappa = 0.0001$

Figure 7: (*cont'd*) Velocity profiles at $T = 0.90$: comparison between numerical results and Eq. (27) for different values of the surface tension parameter κ .

4. Correction force term: reduction of the spurious interface velocity

To eliminate the spurious term in the mass equation (25), we consider a supplementary force term

$$F_{i\beta}^\nu = \frac{\psi}{\rho} [-\partial_\beta(e_{i\gamma}A_\gamma) + (u_\gamma\partial_\beta + u_\beta\partial_\gamma)A_\gamma] \quad (28)$$

where

$$A_\gamma = \chi c^2 \partial_\gamma \rho + \partial_\delta(\rho u_\gamma u_\delta) \quad (29)$$

After introduction of the correction force term (28), the LB equations (24) become

$$\begin{aligned} \mathbf{e}_i \cdot \nabla f_i(\mathbf{x}, t) - \psi e_{i\beta} e_{i\gamma} \partial_\beta \partial_\gamma f_i(\mathbf{x}, t) &= -\frac{1}{\tau} [f_i(\mathbf{x}, t) - f_i^{eq}(\mathbf{x}, t)] + \\ \frac{1}{\chi c^2} f_i^{eq} [e_{i\beta} - u_\beta(\mathbf{x}, t)] [F_\beta + F_{i\beta}^\nu] &\quad (i = 0, 1, \dots, \mathcal{N}) \end{aligned} \quad (30)$$

Introduction of the correction term cancels the spurious velocity term and allows the recovery of the correct mass equation in the stationary case. This is easy to see after calculating the sum

$$\begin{aligned} \sum_i \frac{1}{\chi c^2} f_i^{eq} (e_{i\beta} - u_\beta) F_{i\beta}^\nu &= \\ \sum_i \frac{1}{\chi c^2} \frac{\psi}{\rho} f_i^{eq} (e_{i\beta} - u_\beta) [-\partial_\beta(e_{i\gamma}A_\gamma) + (u_\gamma\partial_\beta + u_\beta\partial_\gamma)A_\gamma] &= \\ -\psi \partial_\beta A_\gamma \delta_{\beta\gamma} = -\psi \chi c^2 \partial_\beta [\partial_\beta \rho + \partial_\delta(\rho u_\beta u_\delta)] &\quad (31) \end{aligned}$$

Moreover, the introduction of the correction force term does not alter the momentum equation since

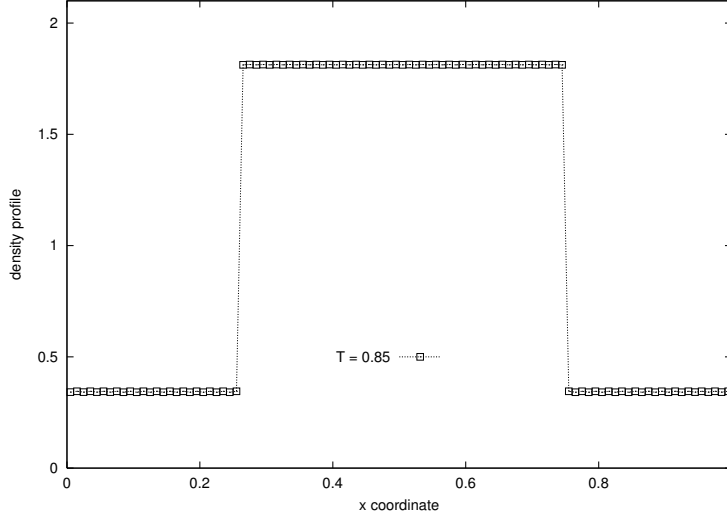
$$\begin{aligned} \sum_i \frac{m}{\chi c^2} \frac{\psi}{\rho} f_i^{eq} e_{i\alpha} (e_{i\beta} - u_\beta) [-\partial_\beta(e_{i\gamma}A_\gamma) + (u_\gamma\partial_\beta + u_\beta\partial_\gamma)A_\gamma] &\simeq \\ -\psi [\delta_{\alpha\beta} u_\gamma + \delta_{\beta\gamma} u_\alpha + \delta_{\alpha\gamma} U_\beta] \partial_\beta A_\gamma + \psi \delta_{\alpha\beta} [u_\gamma \partial_\beta + u_\beta \partial_\gamma] A_\gamma &+ \\ \psi \delta_{\alpha\gamma} \partial_\beta A_\gamma &= 0 \end{aligned} \quad (32)$$

In the 1D case there is no need for Cartesian indices and the expression (28) of the correction force term becomes

$$F_i^\nu = -\frac{\psi}{\rho} (e_i - 2u) [\chi c^2 \nabla^2 \rho + \nabla^2(\rho u^2)] \quad (33)$$

The following formula is used to compute the effect of the Laplace operator on a function f (e.g., ρ or ρu^2) defined in the nodes x of the 1D lattice:

$$\nabla^2 f(\mathbf{x}, t) = \frac{2}{\chi(\delta s)^2} \left[\sum_{i=0}^{i=\mathcal{N}} w_i f(\mathbf{x} + \mathbf{e}_i \delta s/c, t) - f(\mathbf{x}, t) \right] \quad (34)$$

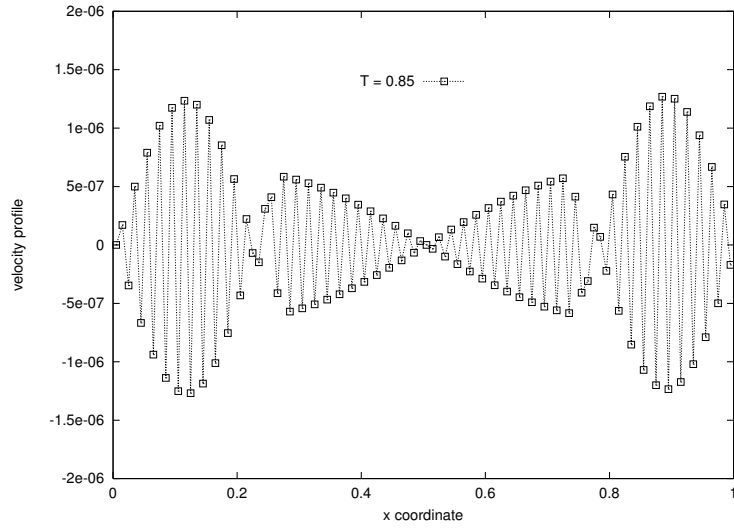


a: density profile

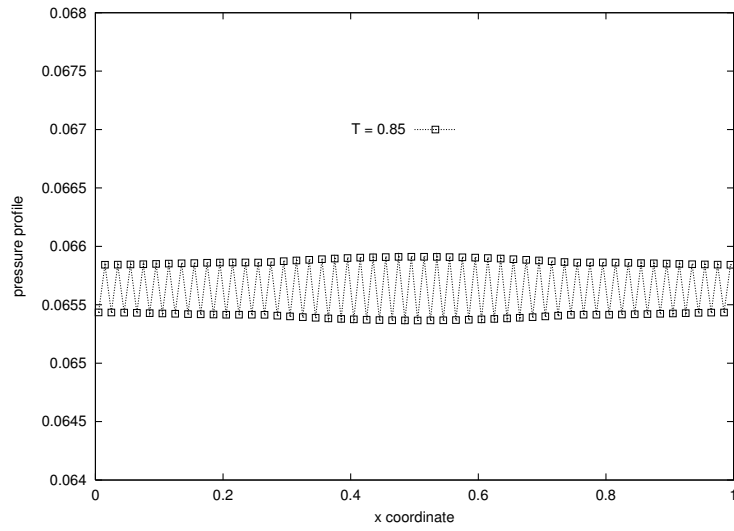
Figure 8: Profiles recovered using the correction force term (28) for $T = 0.85$ and $\kappa = 0$.

Simulations done with the correction force term (28) included in the LB evolution equations give sharp density profiles for $\kappa = 0$ (Figure 8a), as expected. The spurious velocity is no longer present in the interface region. A wiggly profile of the local velocity is still observed (Figure 8b), but the amplitude of the oscillations are several orders of magnitude smaller than the typical value of the spurious velocity arising in the interface region when using the uncorrected upwind scheme. Also the pressure profile recovered for $\kappa = 0$ is quite flat on the whole lattice, although wiggles of very small amplitude are still present (Figure 8c).

As previously observed during simulations with the uncorrected upwind scheme, increasing the surface tension always helps to stabilize the system for lower values of the temperature when the correction force term is considered in the LB evolution equations (Figure 9). However, the phase diagrams recovered using the corrected force term (Figure 9) are closer to theoretical results than the phase diagrams derived with the bare upwind scheme (Figure 6). For large values of the surface tension parameter κ , the overlapping of the left and right interfaces is still present for temperatures close to the critical point, but the plateau is clearly defined in both high and low density phases for lower temperatures (Figure 10). The velocity profile recovered for $T = 0.50$ and $\kappa = 0.0001$ is similar to the one shown in Figure 6b, but the amplitude of the oscillations is significantly reduced (2.0×10^{-14}) because of the stabilization effect of the surface tension.

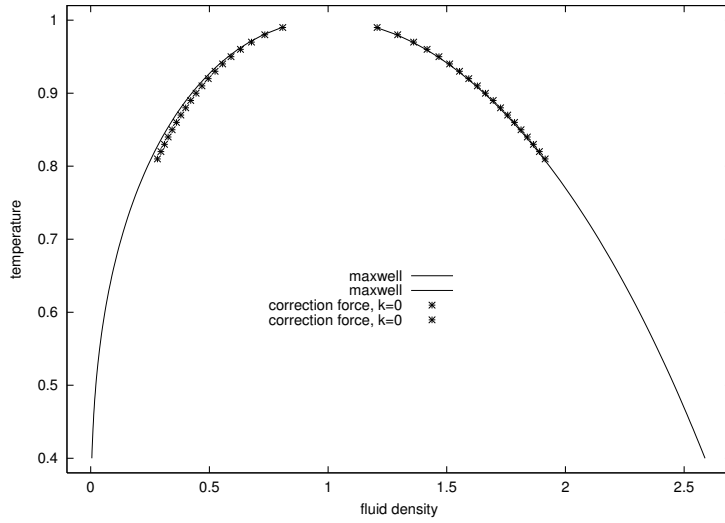


b: velocity profile

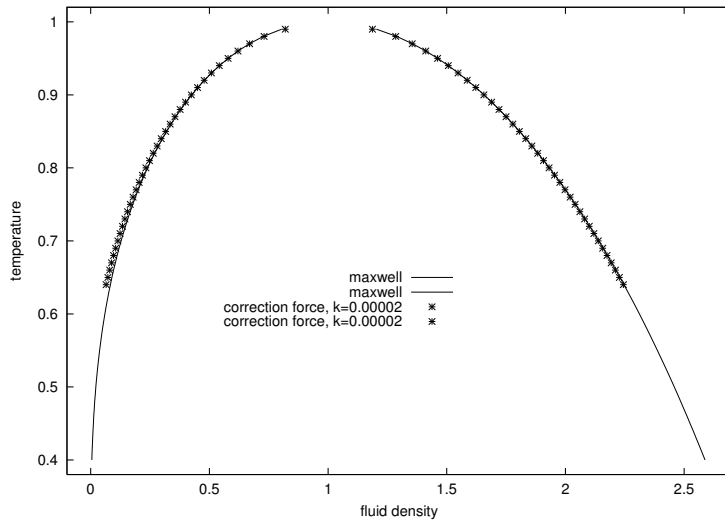


c: pressure profile

Figure 8: (*cont'd*) Profiles recovered using the correction force term (28) for $T = 0.85$ and $\kappa = 0$.



a: $\kappa = 0$



b: $\kappa = 0.00002$

Figure 9: Phase diagram recovered with the correction force term (28).

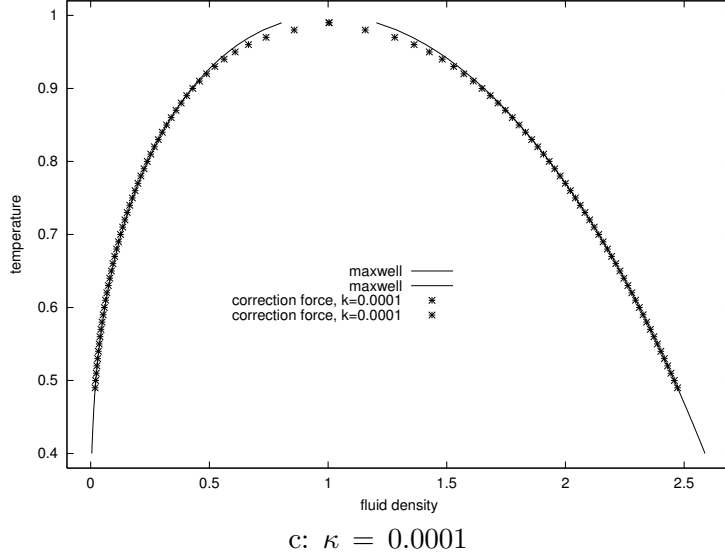
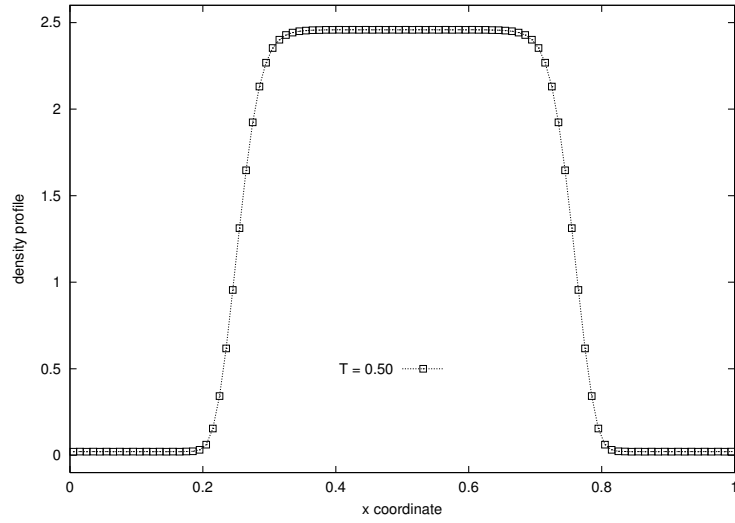


Figure 9: (*cont'd*) Phase diagram recovered with the correction force scheme (28).

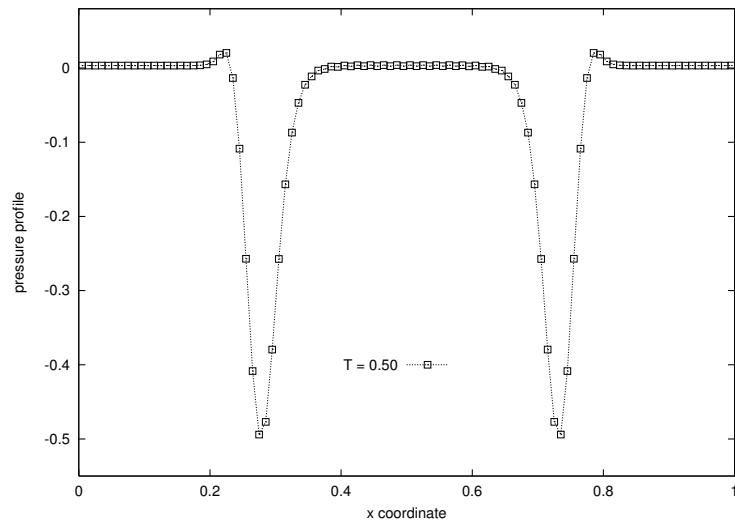
5. Conclusions

The first order upwind finite difference scheme used for the operator $\mathbf{e}_i \cdot \nabla$ in the LB evolution equations (7) generates the spurious velocity in the interface region of liquid - vapor systems. The magnitude of the spurious velocity is related to the density gradient through Eq. (27). Consequently, the spurious velocity is reduced by the surface tension.

A correction force term (28) is suggested to reduce the spurious velocity. Introduction of this term in the LB evolution equations allows to get sharp interfaces when the value of the surface tension parameter vanishes. Moreover, the phase diagram of the liquid - vapor system becomes closer to the theoretical one derived using the Maxwell construction.



a: density profile



b: pressure profile

Figure 10: (*cont'd*) Profiles recovered using the correction force term (28) for $T = 0.50$ and $\kappa = 0.0001$.

References

- [1] D. H. Rothman and S. Zaleski, *Lattice Gas Cellular Automata: Simple Models of Complex Hydrodynamics* (Cambridge University Press, Cambridge, 1997).
- [2] B. Chopard and M. Droz, *Cellular Automata Modeling of Physical Systems* (Cambridge University Press, Cambridge, 1998).
- [3] D. A. Wolf - Gladrow, *Lattice Gas Cellular Automata and Lattice Boltzmann Models* (Springer Verlag, Berlin, 2000).
- [4] S. Succi, *The Lattice Boltzmann Equation for Fluid Dynamics and Beyond* (Clarendon Press, Oxford, 2001).
- [5] K. Huang, *Statistical Mechanics* (John Wiley and Sons Inc., New York, 1963).
- [6] P. L. Bhatnagar, E. P. Gross and M. Krook, *Phys. Rev.* **94**, 5111 (1954).
- [7] V. Sofonea and R. F. Sekerka, *Physica A* **299**, 494 (2001).
- [8] X. He, X. Shan and G. Doolen, *Phys. Rev. Lett.* **57**, R13 (1998).
- [9] R. R. Nourgaliev, T. N. Dinh, T. G. Theofanous and D. Joseph, *Int. J. Multiphase Flow* **29**, 117 (2003).
- [10] X. He and L. S. Luo, *Phys. Rev. E* **55**, R6333 (1997).
- [11] X. He and L. S. Luo, *Phys. Rev. E* **56**, 6811 (1997).
- [12] L. S. Luo, *Phys. Rev. E* **62**, 4982 (2000).
- [13] V. Sofonea and R.F. Sekerka, *J. Comput. Phys.* **184**, 422 (2003).
- [14] Y. H. Qian, D. D'Humières and P. Lallemand, *Europhys. Lett.* **17**, 479 (1992).
- [15] A. Cristea and V. Sofonea, *Proc. Romanian Acad. Series A: Mathematics, Physics, Technical Sciences, Information Science* **3**, 87 (2002).
- [16] A. Cristea and V. Sofonea, *Proc. Romanian Acad. Series A: Mathematics, Physics, Technical Sciences, Information Science* **4**, 59 (2003).
- [17] D. Kondepudi and I. Prigogine, *Modern Thermodynamics: From Heat Engines to Dissipative Structures* (John Wiley and Sons Inc., New York, 1998).
- [18] N. Cao, S. Chen, S. Jin and D. Martinez, *Phys. Rev. E* **55**, R21 (1997).
- [19] Y. Chen, S. Teng, T. Shukuwa and H. Ohashi, *Int. J. Mod. Phys. C* **9** 1383 (1998).
- [20] S. Teng, Y. Chen and H. Ohashi, *Int. J. Heat and Fluid Flow* **21**, 112 (2000).